International Journal of Environmental Sciences
ISSN: 2229-7359
Vol. 10 No. 4, 2024
https://theaspd.com/index.phpa

Optimized DNetCNN Framework for Brain Tumour Segmentation and Classification Using MRI Images

Kiranmai Kollipara[1], Dr. Surendra Reddy Vinta[2]
[1]Research Scholar, SCOPE, VIT-AP University, Amaravati, Andhra Pradesh, India
kiranmai.23phd7101@vitap.ac.in
[2]Associate Professor, SCOPE, VIT-AP University, Amaravati, Andhra Pradesh, India
surendrareddy.vinta@vitap.ac.in

Abstract
The primary cause of brain illnesses is irregular brain cell proliferation, which can harm the structure of the brain and ultimately result in malignant brain cancer. Using a computer-aided diagnostic system to enable an early diagnosis and immediate therapy involves dealing with difficulties, foremost among which is the precise identification of various diseases using magnetic resonance imaging (MRI) scans. This research proposes a new Darknet Convolutional Neural Network (DNetCNN) framework for accurate diagnosis of pituitary, meningioma, and glioma, as well as a two-step preprocessing method to improve the quality of MRI images. The relevant features are extracted using the ResNet152V2 technique to accurate the ground-truth segmentation of tumours. Finally, to improve the classification accuracy using the Enhanced Rat Swarm Optimization Algorithm (ERSOA). An analytical comparison is made between the proposed framework and other models covered in this study. Tested on a dataset comprising MRI pictures, an exceptional competitive accuracy of 99.78% is obtained, with 99.78% accuracy in recognizing gliomas, 99.86% accuracy in detecting meningiomas, 99.68% accuracy in detecting pituitary tumours, and 99.80% accuracy in identifying normal images. The proposed architecture's resilience is demonstrated by experimental results, which have also quickly improved the accuracy of brain disease diagnosis.
Keywords: *MRI brain tumour; detection; feature extraction; classification; enhanced rat swarm optimization algorithm; pre-processing; noise removal.*

1. INTRODUCTION

The most important organ in the human body with the most intricate structure is the brain. The skull covering that envelops the brain makes it challenging to examine its behaviors and makes disease identification more challenging. Although brain disease is distinct from diseases affecting other parts of the body, it can be brought on by abnormal cell proliferation, which leads to the eventual destruction of the brain's structure and the development of brain cancer [1-3]. Nonetheless, World Health Organization (WHO) research estimates that 9.6 million people worldwide lost their lives to cancer in 2018. Likewise, between 30 to 50 percent of people with initial cancer diagnoses. Brain cancer is one of the deadliest cancer kinds. Accordingly, the data indicates that 17,760 adult deaths in 2019 were attributed to brain tumours. Timely diagnosis is essential due to the severe circumstances, aberrant growth, and complexity of brain structure associated with cancer [4, 5]. High-quality brain pictures obtained from magnetic resonance imaging (MRI) are highly valuable for tumour analysis. The MRI method is particularly important for brain imaging because it offers a special means of achieving the finest possible visualization of maximum contrast and spatial determination.

The growing advances in medical image processing have made brain tumours and their analysis more interesting. The fundamental idea behind these advancements is the use of hierarchical feature representations that are exclusively learnt from data, as opposed to features that are manually created using domain-specific expertise [6, 7]. Similar to this, some works have recently proposed models or frameworks that highlight the brain tumour zone. In medical image processing, brain tumour segmentation is required and is typically controlled by characteristics including low contrast, noise, and missing boundaries. When evaluating brain images, MRI segmentation that makes use of learning algorithms and pattern recognition technologies works incredibly well [8-10]. In technical terms, the approach is a parametric model that takes into account the functions chosen by the density function.

When it comes to the diagnosis, planning, and assessment of cancer treatment, early detection, accurate grading, and categorization of brain tumours are essential. Despite the advancements in medical technology, histological examination of biopsy specimens remains the primary method for the recognition, categorization, and grading of brain tumours [11-13]. The ultimate diagnosis is typically reached via a pathological examination, clinical assessment, and interpretation of imaging modalities like CT or MRI. The main drawbacks of this diagnostic technique are well known to be their intrusiveness,

length of time, and susceptibility to sampling errors [14, 15]. Increasing the diagnostic skills of radiologists and doctors can assist reduce the time needed for the right diagnosis by using computer-aided completely automated detection and diagnosis technologies that strive to produce quick and accurate conclusions by professionals. To overcome the issues in the existing methods, propose a novel technique to detect and classify brain tumour disease. The key contribution of this research is,

- Initially, the input image is collected from Brain MRI images to perform pre-processing processes. In this step, perform the noise reduction from the input image and enhance the contrast of the image to make it easy to extract the attributes from the picture.
- To obtain the attributes from the pre-processed picture using the ResNet152 technique such as texture, shape, and colour features to recognize the tumour from brain images.
- To segment the ground truth and lesion area of the tumour in a given brain image using the Dense-U-Net model. Finally, classify the tumours into their category using the Darknet Convolutional Neural Network, which the dataset contains four types of tumours.
- To improve the classification accuracy, employ the Enhanced Rat Swarm Optimization Algorithm. An analytical comparison is made between the proposed framework and other models covered in this study.

This is how the rest of the essay is organized. Section 2 discusses the relevant research on deep learning-based brain tumour categorization. In Section 3, the proposed approach and its elements are discussed in detail. Section 4 explains the experimental approach. In Section 5, the work is examined and recommendations for more research are made.

2. LITERATURE SURVEY

In this section, analyzed and revised some previous studies on brain tumour detection and classification topics. Shuai et al. [16] suggested a deep wavelet autoencoder system called the "DWAE model," which is used to classify input data slices as either normal or pathological tumours. Using a high pass filter, the MRI pictures' heterogeneity and integration with the input images were demonstrated in this paper. It smoothed the raw MR brain pictures and highlighted edges to improve the quality of the output slices. Next, since the thresholding cluster matched pixels with the input MR picture, used the 4-connected seed growth approach. The suggested deep wavelet auto-encoder model yields two two-layer segments from the segmented MR image slices.

Five steps make up the suggested technique by Maqsood et al. [17]. First, the pictures are identified utilizing a linear contrast stretching technique. The third phase involves training a modified MobileNetV2 framework via transfer learning and employing it for feature extraction. The fourth phase involved selecting the optimal features using a multiclass support vector machine (M-SVM) in conjunction with an entropy-based controlled technique. In the last stage, meningioma, glioma, and pituitary pictures are identified by the application of M-SVM for brain tumour categorization.

Rammurthy & Mahesh [18] presented Whale Harris Hawks optimization (WHHO), an optimization-driven method for MR image-based brain tumour diagnosis. Here, rough set theory and cellular automata are used for segmentation. Furthermore, the tumour size, Mean, Local Optical Oriented Pattern (LOOP), Variance, and Kurtosis are derived from the segments. Furthermore, a Deep CNN is used to detect brain tumours; the network is trained using the suggested WHHO. The Harris Hawks Optimization (HHO) and Whale Optimization (WOA) algorithms are integrated to create the suggested WHHO.

Vankdothu & Hameed [19] suggested a detection and classification automated technique. The suggested approach is broken down into four categories: feature extraction, picture categorization, image segmentation, and MRI image preparation. An adaptive filter is used in the picture preprocessing step to eliminate the MRI picture's noise. The GLCM is employed for attribute extraction, while the improved K-means clustering (IKMC) technique is used for image segmentation. Following the extraction of features from MRI pictures classified the various image types—gliomas, meningiomas, non-tumours, and pituitary tumours—using a deep learning model. Recurrent convolutional neural networks (RCNN) were utilized in the classification procedure. When classifying brain images from a given input dataset, the suggested strategy yields superior results. An efficient fusion-based brain tumour identification and segmentation method was suggested by Preethi & Aishwarya [20] to help with accurate brain tumour identification. DWT and the new fusion rule are first used to fuse the input picture. Extracting the GLCM features comes after the fusion procedure. Next, use an ODNN to categorize the brain pictures into normal and pathological categories. In this case, the SMO technique is utilized to choose the DNN network weights optimally.

Aurna et al. [21] suggested a method for the accurate categorization of brain tumours that makes use of a two-stage feature ensemble using deep Convolutional Neural Networks (CNN). A dataset that combines all three distinct Magnetic Resonance Imaging (MRI) datasets is taken into consideration. Based on accuracy, the top classifier is also selected from a set of five classifiers. PCA is utilized to choose the most significant attributes from the retrieved characteristics, which are then fed into the classifier. There are certain restrictions on the identification and categorization of brain tumours currently in use. The Figshare dataset, which is unbalanced and influences the performance of classification algorithms, is used to validate the majority of the approaches. Therefore, methods for classifying brain tumours need to be validated using a different balanced dataset. In its conventional form, machine learning requires domain expertise. The system is less efficient when features are extracted manually because it takes time and effort. However, because deep learning—and CNN in particular—needs a large amount of data for training, using it in medical imaging is difficult. However, by utilizing powerful classification applications based on convolutional layers and automated feature extraction, deep TL-based algorithms can circumvent these shortcomings. An automatic categorization system for multiclass brain tumour magnetic resonance images is proposed in this paper. This is a more intricate and challenging task than basic binary classification. To demonstrate the effectiveness of the best system in recognizing brain cancers, also compared it with other techniques.

3. PROPOSED METHODOLOGY

In medical imaging and healthcare, identifying and classifying brain tumours is essential. It entails classifying brain tumours according to their type, size, location, and other attributes by employing a variety of imaging modalities, including CT, MRI, and others. This research proposes a new DL-based approach to detect and categorize brain tumour disease. It involves five steps to process. To begin pre-processing, the input image is first gathered from Brain MRI scans. To facilitate the extraction of features from the image, apply noise reduction on the input image and adjust contrast in this step. Then, to identify the tumour from brain scans, extract features including texture, shape, and color from the pre-processed image using the ResNet152 approach. Afterwards, use the Dense-U-Net model to segment the ground truth and tumour lesion area in the provided brain picture.

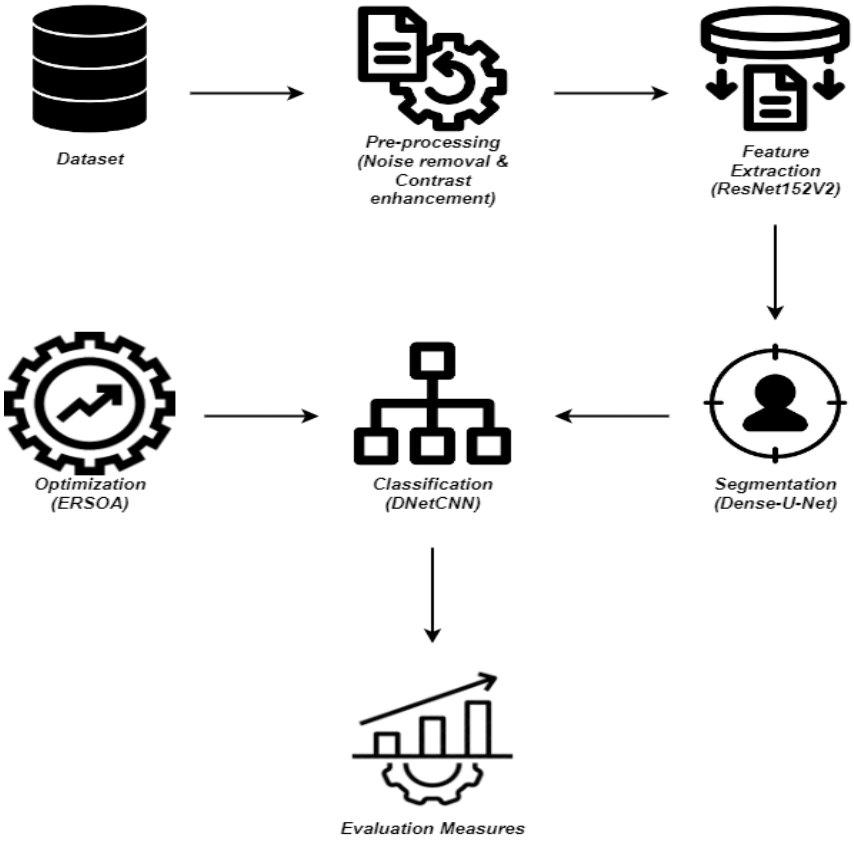

Fig. 1. Architecture of proposed method.

Lastly, use the Darknet Convolutional Neural Network to categorize the tumour into the appropriate category. This dataset includes four different types of cancers. Use the Enhanced Rat Swarm Optimization Algorithm to increase the classification accuracy. Fig. 1 demonstrates the structure of the proposed system.

3.1. Pre-processing

In this pre-processing stage, median filtering has been used to eliminate noise from the contrast-enhanced picture. The proposed approach makes use of median filtering, which examines the image pixel by pixel and replaces each value with the median value of the nearby pixel. The size of the window determines the neighbor's pattern. This piece makes use of a 3 × 3 neighborhood window size. The median filter is applied on I^1 as:

$$I^2(i,j) = \text{median}\{I^2(i,j)|(i,j) \in w\} \quad (1)$$

Where I^2 is the outcome of the median filtering and w is the size of the window.

By varying the saturation and contrast, traditional haze-removal methods seek to create a high-quality rebuilt image. The haze reduction process can significantly improve the scene's visibility in the picture. This work applied a hybrid method of local-global transformation and haze removal for contrast improvement. This method's mathematical description is as follows: Imagine that Δ represents the full image database with N pictures. The final improved picture is $CF(x,y)$, and let $I(x,y)$ be the original picture with dimensions N × M × 3. Initially, used an approach to reduce haze in the image that was based on the dark channel. The following is a mathematical definition of the haze reduction process:

$$H(x) = y(x)t(x) + L(1 - t(x)) \quad (2)$$

where Y stands for scene radiance, t(x) for the transmission map, H for the observed intensity value, and L for ambient light. By estimating the transmission map and atmospheric light, the dehazing method in use retrieves the scene radiance Y in the following manner:

$$Y(x) = \frac{(H(x)-\alpha)}{(\max(t(x),t_o))} + \alpha \quad (3)$$

After that, the resulting $y(x)$ is used to calculate an image's global contrast using the following formula:

$$g_o = (1 + C_k) \times (g_i - k_{mean}) + \sigma \quad (4)$$

where g_o is the final global contrast picture, σ is the standard deviation of $Y(x)$, kmean is the global mean value of $Y(x)$, g_i is the input pixel value of $Y(x)$, and C_k is the global contrast gain factor. In the second phase, the following mathematical function to calculate the haze reduction image's local contrast:

$$L(x,y) = \emptyset(x,y) + \frac{LC}{\sigma(i,j)+\alpha} \times [\emptyset(x,y) - \mu(x,y)] \quad (5)$$

The dehazed picture $Y(x)$ is represented by the grayscale pixel $\emptyset(x,y)$, where LC stands for local contrast, α for a tiny parameter value, and $\mu(x,y)$ for the dehazed image's mean value, respectively. Lastly, utilized the following mathematical formula to combine the local and global contrast resulting images into a single image, producing the final improved image. The improved image in its final form is $CF(x,y)$.

$$CF(x,y) = [g(x,y) + L(x,y) - I(x,y)] \quad (6)$$

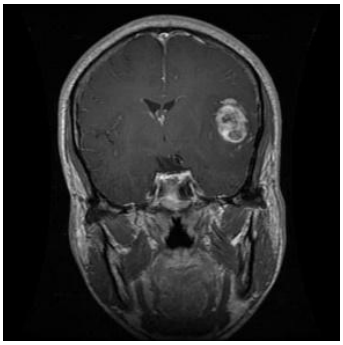

(a) Original picture

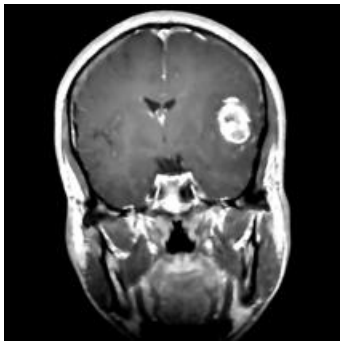

(b) Contrast-enhanced picture

(c) Histogram of the original picture

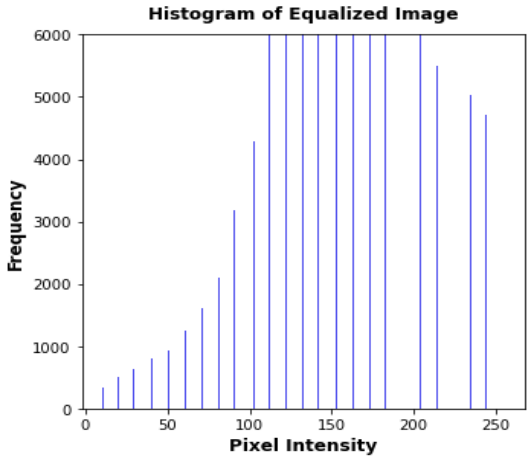

(d) Histogram of equalized picture

Fig. 2. Sample histogram outcome of the original picture and contrast-enhanced image

Fig. 2 demonstrates the outcome of the enhancement histogram of the original and contrast enhancement image.

3.2. Feature Extraction

After performing pre-processing on the input image, using the ResNet152V2 technique to retrieve the attributes such as texture, colour, and shape to enhance the classification performance. A CNN variant called residual learning network (ResNet) efficiently facilitates deeper network learning. ResNet used residual learning to get over the deeper networks' vanishing/exploding gradients issue. When the input and output dimensions of the stacked convolutional blocks match, shortcut or skip connections can be added to the residual network. In a 2-layer stack, a skip connection adds the first convolution block's input to the subsequent convolution block's output. Shortcuts can use 1*1 convolution to project to match dimensions when the input and output sizes disagree, or they can pad the output with zero. To solve the degradation difficulties, this aids in the explicit reformulation of the layers using identity mapping. To alleviate the disappearing gradient issue, shortcut connections permit the gradient to pass through itself. Improved performance was demonstrated in bottleneck-based ResNet topologies using parameter-less identity shortcuts. To improve accuracy in the ImageNet challenge, the 152-layer ResNet used 3-layer bottlenecks to replace the 2-layer blocks of the Resnet-34. ResNet152V2 utilizes the original ResNet152 as a pre-activated rectified linear unit (RELU).

The basic equation of a residual block is as follows.

$$y_1 = f(x_1, w_1) + h(x_1), x_2 = f(y_1) \quad (7)$$

Here, $w_1, w_2, \ldots, i$ stands for the weight of the particular residual unit, and f, $x_1, x_2, \ldots, i$ for the residual function, designate the ith residual unit. Now, if x_2 is less than y_1, then

$$x_2 = x_1 + f(x_1, w_1) \quad (8)$$

$$x_3 = x_2 + f(x_2, w_2) = x_1 + f(x_1, w_1) + f(x_2, w_2) \quad (9)$$

$$x_4 = x_3 + f(x_3|w_3) = x_1 + f(x_1, w_1) + f(x_2, w_2) + f(x_3, w_3) \quad (10)$$

$$x_i = x_1 + \sum k = 1^{i-1} f(x_k, w_k) \quad (11)$$

Additionally, Eq. (11) impacts the backpropagation as defined by Eq. (12).

$$\frac{\partial \emptyset}{\partial x_1} = \frac{\partial \emptyset}{\partial x_i} \cdot \frac{\partial x_i}{\partial x_1} = \frac{\partial \emptyset}{\partial x_i}\left(1 + \frac{\partial}{\partial x_1}\sum k = 1^{i-1} f(x_k, w_k)\right) \quad (12)$$

In this case, the loss function is φ, and all units are capable of rapidly transmitting the signal backwards as well as forwards based on Eqs. (11) and (12). This research addresses the sequential difficulty of the framework by introducing the bi-directional gated recurrent unit (Bi-GRU). The Bi-GRU takes into account the sequences of the data before and after it to minimize noise during processing. With rapid reaction times and efficient extended operation, this model performs more quickly. Ultimately, the Resnet152V2 with BiGRU detects and categorizes network intrusions and produces the result via the last layer.

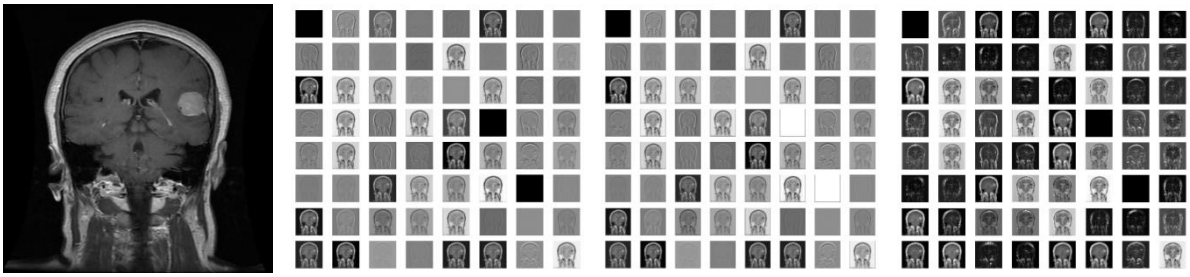

(a) Original Image (b) conv1_conv (c) pool1_pad (d) pool_pool

Fig. 3. Output features of partial convolutional layers.

Fig. 3 shows the feature output of partial convolutional layers.

3.3. Tumor Segmentation

To segment the tumour part in the brain image, utilize the Dense-U-Net model. Convolutional neural networks are capable of extracting high-level information from low-level data and conversely. Enhancing the network's learning capacity is not effectively achieved by the low feature reuse rate; instead, it is more significant to raise the feature use rate rather than deepen the network. A dense module is presented to enhance feature use, where every layer in the dense block is intimately related to every layer before it. Dense-net enhances classification performance by utilizing dense blocks. To finish the convolutional network for semantic segmentation, Dense-Net was expanded and used for scene segmentation. As a result, a Dense U-Net is proposed as the foundation for segmenting brain tumours. Randomly extracted image blocks with a resolution of 48 × 48 were used as training data. The model output, which shows the outcome of tumour segmentation, is the prediction result. A dense network is made up of transition layers, connecting layers, dense blocks, and an extension path.

3.3.1. Dense Block

Residual networks served as an inspiration for the Dense-Net architecture. The primary distinction lies in the fact that Res-Net defines its input for every layer based on the output of the preceding finite layer. Dense-Net uses all of the preceding layers' outputs to characterize each layer's input. Furthermore, every layer's output properties are used as the input for all levels that follow. When the outcome of the layer L is x_L, it is defined as:

$$x_L = H_L([x_0, x_1, \dots, x_{L-1}]) \quad (13)$$

The combination of distinctive layers of layer 0,1,...,L-1 output is represented by the expression $[x_0, x_1, \dots, x_{L-1}]$; H_L is a composite function made up of three modules: batch standardization, a linear correction unit, and a 3*3 convolution layer. The dense part, which has L layers, uses a conversion function to create k feature maps for every layer. The rate of network growth is K. Let's say that the input feature mapping has k_0 channels. This means that the output layer attribute mapping has k channels $k_0 + k \times (L-1)$.

3.3.2. Loss Function

According to the statistical findings, brain tumours make up only 10% of the pixels in fundus imaging. Vascular to non-vascular pixel ratios are drastically out of proportion. Vascular pixels are frequently lost or only partially detected as a result of learning processes that can enter the local minima of the loss function. A class-equilibrium cross-entropy-based loss function. On the other hand, the weight coefficient influences the loss value. The Dice coefficient, which has a range of 0 to 1, is the basis for the new loss function that this method uses. Equation (14) defines the dice coefficient:

$$D = \frac{2\sum_t^N p_t g_t}{\sum_t^N p_t^2 + \sum_t^N g_t^2} \quad (14)$$

Where p_i and g_i represent the expected outcome and ground truth, respectively, and N is the amount of label pixels. The gradients can be produced by differentiating the formula as follows:

$$\frac{\partial D}{\partial p_f} = 2\left[\frac{g_f(\sum_t^N p_t^2 + \sum_t^N g_t^2) - 2p_f(\sum_t^N p_t g_t)}{(\sum_t^N p_t^2 + \sum_t^N p_t^2)^2}\right] \quad (15)$$

3.4. Classification

Following the selection of the most crucial elements, categorize the tumour using a new DL approach called DNetCNN. To increase the categorization accuracy of brain tumours, the DNetCNN structure was incorporated as the initial layer of CNN in the proposed study. The activation function of the darknet structure activates five pooling layers and 19 convolutional layers. Employ the sigmoid activation function

for binary categorization. The activation function Softmax is utilized for multiple classifications. Eq. (16) is used to carry out the 2D convolutional operation for the kernel K and input data X.

$$C(X,K)_{(i,j)} = \sum_r \sum_c K(r,c) \times X \times (i-r, j-c) \quad (16)$$

K: Input matrix containing the step value. The sigmoid function is employed as an activation function in the proposed DNetCNN since the testing dataset, which is a brain tumour, is classified as binary using Equation (17).

$$\text{sigmoid}(h) = \frac{1}{1+e^{-X_i}} \quad (17)$$

There were sixteen convolution layers in the DNetCNN model. One convolutional layer including the convolution and activation procedures was developed in each darknet layer. The same three sequential forms are followed by each of the 4 convolution layers. The input information was standardized by the convolution layer's usual functioning, which shortened the training period. A neuron's ability to activate will keep it from dying. The Maxpool function in the pooling layer was performed out utilizing 2*2. It will optimize the area that the filters were able to employ. From the darknet to the convolution layer, the filter's size changed between 8, 16, 32, and 64. The first layer was the darknet layer, which had a 3*8 filter. Then came pool, DN, then CNN in that order. Filter value 256 was used in the final convolution layer. With accuracy, a brain tumour was classified using the DNetCNN approach. To improve the classification accuracy, employ the Enhanced Rat Swarm Optimization (ERSO) algorithm.

3.5. Optimization

To increase the categorization accuracy, the ERSOA is applied. A new swarm-intelligence algorithm called the Rat Swarm Optimizer was developed in 2021. The following is a detailed description of the RSO's key steps.

Step 1: Setting up the RSO's parameters. The initial values of the various RSO parameters must be assigned at the outset. There are three control parameters and two algorithmic ones in the RSO. Three random values, A, C, and R, represent the control parameters. C falls between [0, 2] and R falls between [1, 5]. Equation (18) is used to initialize the value of A. To regulate the exploration and exploitation capacities during the search process, RSO uses variables A and C.

$$A = R - t \times \left(\frac{R}{T_{max}}\right), \quad t = 1,2,\ldots,T_{max} \quad (18)$$

Step 2: Build the RSO population's initial. In the second stage, generated rat locations, or solution vectors, are added to the RSO population (RP). N determines the quantity of these locations. As shown in Eq. (19), the RSO population is calculated and represented as a two-dimensional matrix of size $N \times d$.

$$RP = \begin{bmatrix} X_{1,1} & X_{1,2} & \cdots & X_{1,d-1} & X_{1,d} \\ X_{2,1} & X_{2,2} & \cdots & X_{2,d-1} & X_{2,d} \\ \vdots & \vdots & \cdots & \vdots & \vdots \\ X_{N-1,1} & X_{N-1,2} & \cdots & X_{N-1,d-1} & X_{N-1,d} \\ X_{N,1} & X_{N,2} & \cdots & X_{N,d-1} & X_{N,d} \end{bmatrix} \quad (19)$$

Step 3: Assessment of fitness. In this phase, the objective method (Xi), $\forall i$ = 1, 2,..., N, is utilized to calculate the fitness value of the rat locations saved in RP. The rat that has the best position in RP, also known as the fittest solution vector, is then chosen and given the name $Xgbest$.

Step 4: Position revision. This step involves two consecutive actions to alter each rat's location in RP: (1) chasing the target, and (2) fighting with the target.

1. Chasing the target. The rat in the greatest place Prey's place is $Xbbet$. According to the characteristics of $Xgbest$, as shown in Eq. (20), the positions of the other rats in RP are updated.

$$\vec{X} = A \cdot \vec{X}_i(t) + \left(\vec{X}^{gbest} - \vec{X}_i(t)\right) \quad (20)$$

In this case, $\vec{X}(t)$ is the ith rat location, t is the current iteration, which accepts values between 1 and $T\,max$, and step 1 explains the parameters A and C.

2. Fighting with target. Every rat's location in RP is updated based on the prey's location, as indicated by Equation (21)

$$\vec{X}_i(t+1) = \left|\vec{X}^{gbest} - \vec{X}\right| \quad (21)$$

where $\vec{X}$ is the modified location determined by utilizing Eq. (21) and $\vec{X}(t+1)$ is the new location of the rat at the ith point.

Step 5: Revise the best and perfect option. This phase involves updating $XgbesH$ with $(t + 1)$ only in cases where $(t + 1)$'s fitness outperforms $XgbesH$. Put differently, given that $((t + 1)) < (Xgbest)$, then $Xgbest = (t + 1)$, for $i \in [1, N]$.

Step 6: Verify the stopping situation. Lastly, until the stop condition is satisfied, steps 4 and 5 are repeated. The work's termination condition is the maximum amount of iterations $Tmax$. The best solution to the optimization problem found thus far is $Xgbest$.

3.5.1. Enhanced RSO (ERSO)

The first step is the random formation of a pool of particles, or solutions. In the search space, each particle possesses information about its position, velocity, and optimal position thus far. Every particle has its position updated based on its velocity. It is repositioned based on both its optimal location and the optimal location that each particle in the swarm found. Eq. (22) can be used to determine each particle's position.

$$\vec{X}_i(t+1) = \vec{X}(t) + \vec{V}(t+1) \quad (22)$$

$$\vec{V}(t+1) = \vec{V}(t) + C_1 \cdot r_1 \cdot \left(\vec{X}_i^{ibest}(t) - \vec{X}(t)\right) + C_2 \cdot r_2 \cdot \left(\vec{X}^{gbest}(t) - \vec{X}(t)\right) \quad (23)$$

In this study, the positions of all the rats in the population as well as each rat's personal best position thus far are used to modify the positions of the rats while they pursue prey, which can be mathematically described using Eq. (24).

$$\vec{X} = A \cdot \vec{X}_i(t) + C \cdot \left(\vec{X}^{gbest}(t) - \vec{X}_i(t)\right) + r_3 \cdot \left(\vec{X}_i^{ibest}(t) - \vec{X}_i(t)\right) \quad (24)$$

The local best location achieved by the ith rat up to iteration t is represented by $\vec{X}lbest\ (t)$, and $U3$ is a random number between 0 and 1. According to the explanation above, the proposed algorithm moves every Rat in the population closer to both the best location for rats overall and for rats as a whole to discover the best solution at each iteration. Note that ERSO is the acronym for the proposed algorithm in this phase.

4. RESULT AND DISCUSSION

The MR imaging dataset description, evaluation metrics, and simulation setup are covered in this section.

4.1. Experimental Setup

Various resources have been used in the model's development. Table 1 illustrates the environmental setup of the proposed system.

Table 1. An environment setup for the proposed model.

Resource	Details
CPU	Core i5 Gen6
GPU	4 GB
RAM	8 GB
Software	Python

4.2. Dataset Details

Brain Tumor Classification (MRI) from the Kaggle license CCO: Public Domain is the dataset used to simulate the performance of the proposed method. There are 3264 MRIs in all. The training and testing datasets are the two distinct categories into which the dataset is divided. The MRIs in the training dataset are divided into four classes: brain MRIs with gliomas, meningiomas, no tumours, and pituitary tumours are represented by the numbers 826, 822, 395, and 827, respectively. In the testing dataset, brain MRIs for glioma, meningioma, no tumour, and pituitary tumour are represented by 100, 115, 105, and 74, respectively. Fig. 4 displays a sample of the datasets.

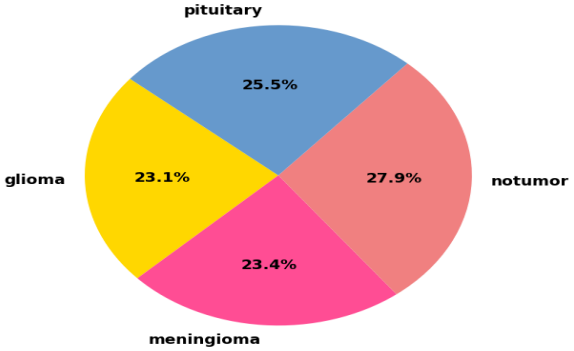

Fig. 4. Datasets distributed values of Dataset.

4.3. Evaluation Metrics

The performance of each deep neural network was assessed in this research using recall, f1-score, precision, and accuracy. Using the following formulas, all performance measurements were determined:

$$\text{Accuracy} = \frac{\text{TP+TN}}{\text{TS}} \quad (25)$$

$$\text{Precision} = \frac{\text{TP}}{\text{TP+FP}} \quad (26)$$

$$\text{Recall} = \frac{\text{TP}}{\text{TP+FN}} \quad (27)$$

$$\text{F1} - \text{Score} = 2 \cdot \frac{\text{Precision} \times \text{Recall}}{\text{Precision+Recall}} \quad (28)$$

4.4. Experiment on Dataset

This section displays the performance of the proposed approach on this dataset. The proposed method assesses a few measures to adjust the parameters. To increase the effectiveness of the proposed procedure, first, clean up the noise from the input images before normalizing them. There are four different kinds of brain tumours in this dataset. To categorize these kinds, apply the proposed approach.

Input Image	Noise Removal	Contrast Enhancement	Segmentation	Classification
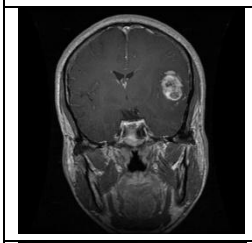	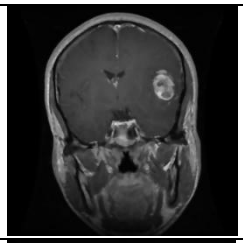	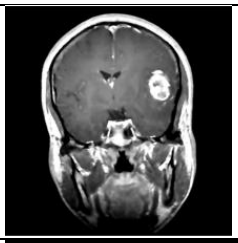	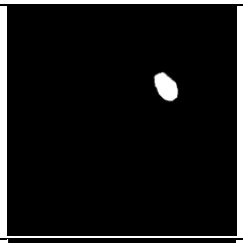	Glioma
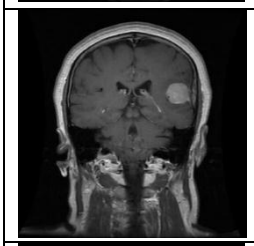	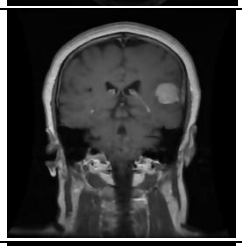	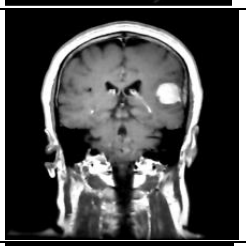	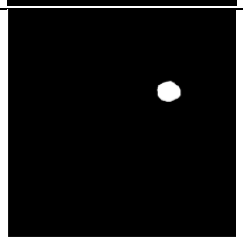	Meningioma
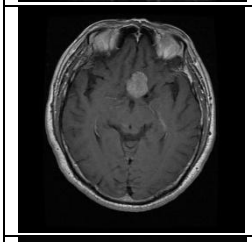	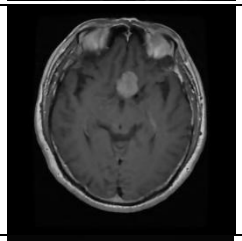	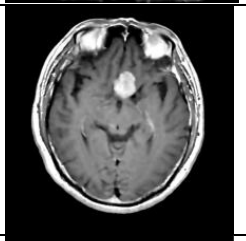	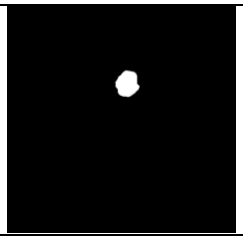	Pituitary
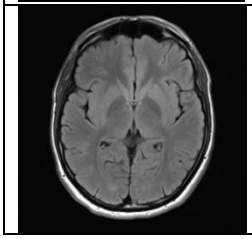	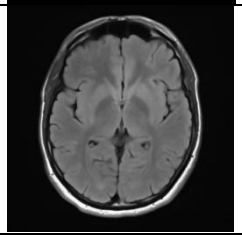	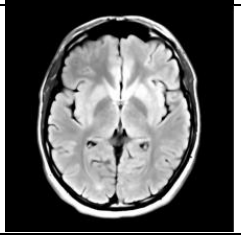	It's an unaffected image.	No tumours

Fig. 5. The proposed methodology performs on the dataset, (a) input picture, (b) noise removed picture, (c) contrast-enhanced picture, (d) segmented picture, (e) classification type.

Fig. 5 shows the outcome of the proposed methodology.

4.4.1. Multi-class classification of the proposed method on a dataset

This section evaluates the brain disease classification system's performance using a dataset. The proposed system was created to classify four different types of brain tumours in the dataset. The performance metrics recall, accuracy, f1-score, and precision for these different types of brain tumours are shown in Table 2 below. The performance metrics of a dataset with four different levels of brain tumours—glioma, meningioma, pituitary, and no tumours—both with and without optimization are displayed in Table 2. For every lesson, precision, recall, F1-score, and accuracy were assessed.

Table 2. Performance Metrics for four different levels of a brain tumour in the dataset.

Classes	Without Optimization	With Optimization

	Precision (%)	Recall (%)	F1-score (%)	Accuracy (%)	Precision (%)	Recall (%)	F1-score (%)	Accuracy (%)
Glioma	99.12	99.34	99.22	99.32	99.69	99.76	99.72	99.78
Meningioma	99.24	99.43	99.33	99.18	99.59	99.48	99.53	99.86
Pituitary	99.16	99.12	99.13	99.21	99.74	99.79	99.76	99.68
No tumours	99.32	99.25	99.28	99.13	99.63	99.85	99.73	99.80

Glioma demonstrated precision, recall, F1-score, and accuracy of 99.12%, 99.34%, 99.22%, and 99.32%, respectively, without optimization. These metrics increased to 99.69%, 99.76%, 99.72%, and 99.78% after optimization. Similar patterns were observed in meningioma, where optimization resulted in increases in precision, recall, F1-score, and accuracy from 99.24%, 99.43%, 99.33%, and 99.18% to 99.59%, 99.48%, 99.53%, and 99.86%, respectively. With optimization, pituitary and no tumours also had increases in their performance metrics; all classes showed considerable gains in accuracy, precision, recall, and F1-score.

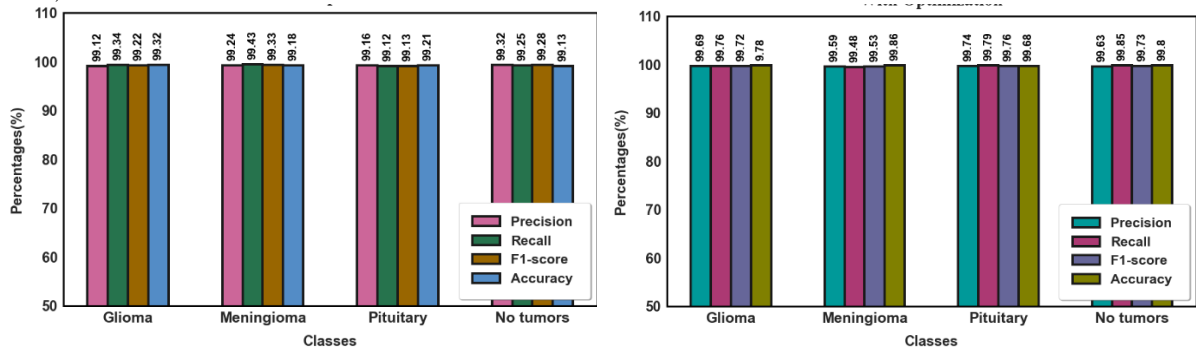

(a) (b)

Fig. 6. Multi-class classification for a dataset using the proposed methodology: (a) without optimization, (b) with optimization.

The proposed method results for each class mentioned in Table 2. Fig. 6 demonstrates the performance of the proposed method on the dataset without optimization and with optimization values for accuracy, f1-score, recall, and precision metrics. A detailed comparison between the proposed approach and other well-known techniques using the dataset is shown in Table 3.

Table 3. The comparison of the proposed method with previous approaches on the dataset.

Methods	Precision (%)	Recall (%)	F1-score (%)	Accuracy (%)
ResNet-50	87	93	90	89
VGG-19	94	93	93	93
Inception-V3	77	71	74	75
ResNet-101	74	74	73	74
Proposed Method	99.66	99.72	99.68	99.78

Preliminarily, the proposed method shows superiority in accuracy, F1-score, recall, precision, and performance compared to all previous methods in all parameters. 87% precision, 93% recall, 90% F1-score, and 89% accuracy are impressive findings for ResNet-50. 94% precision, 93% recall, 93% F1-score, and 93% accuracy are even better than what VGG-19 shows.

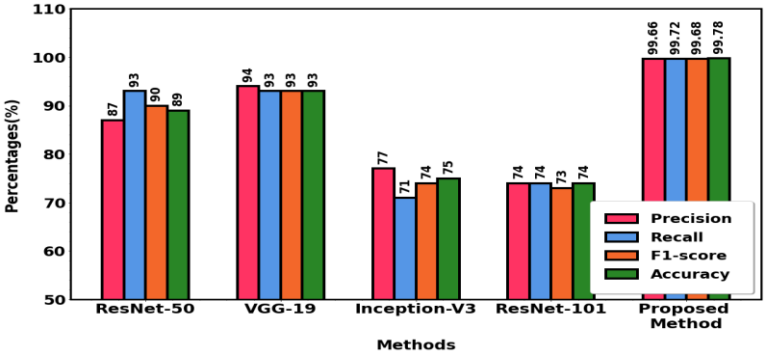

Fig. 7. Comparison of the proposed method with previous approaches in the dataset.

Despite displaying outstanding outcomes, Inception-V3 and ResNet-101 are inferior to the proposed approach and the previously described models. It sets a new standard with outstanding precision (99.66%), recall (99.72%), F1-score (99.68%), and accuracy (99.78%). Fig. 7 shows the proposed and existing methods comparison of the dataset.

4.5. Overall comparison of the proposed method with previous approaches

An overall comparison of previously published and proposed approaches for accuracy (%) in a variety of classification tasks is given in Table 4. Maqsood et al. [17] provided M-SVM, which achieved an accuracy of 97.47%, whereas Shuai et al. [16] introduced DWAE, which achieved an accuracy of 99.3%. Vankdothu & Hameed [19] used RCNN to achieve an accuracy of 95.17%, while Rammurthy & Mahesh [18] offered WHHO-based DeepCNN with an accuracy of 81.6%. Aurna et al. [21] applied DCNN with an accuracy of 98.96%, while Preethi & Aishwarya [20] presented ODNN with an accuracy of 93%.

Table 4. Overall comparison of proposed and previous methods in the literature.

Reference	Method	Accuracy (%)
Shuai et al. [16]	DWAE	99.3
Maqsood et al. [17]	M-SVM	97.47
Rammurthy & Mahesh [18]	WHHO-based DeepCNN	81.6
Vankdothu & Hameed [19]	RCNN	95.17
Preethi & Aishwarya [20]	ODNN	93
Aurna et al. [21]	DCNN	98.96
Proposed Method	Optimized DNetCNN	99.78

With an outstanding accuracy of 99.78%, the proposed approach, Optimized DNetCNN, surpasses all prior methods, demonstrating its supremacy in classification tasks when compared to current approaches in the literature.

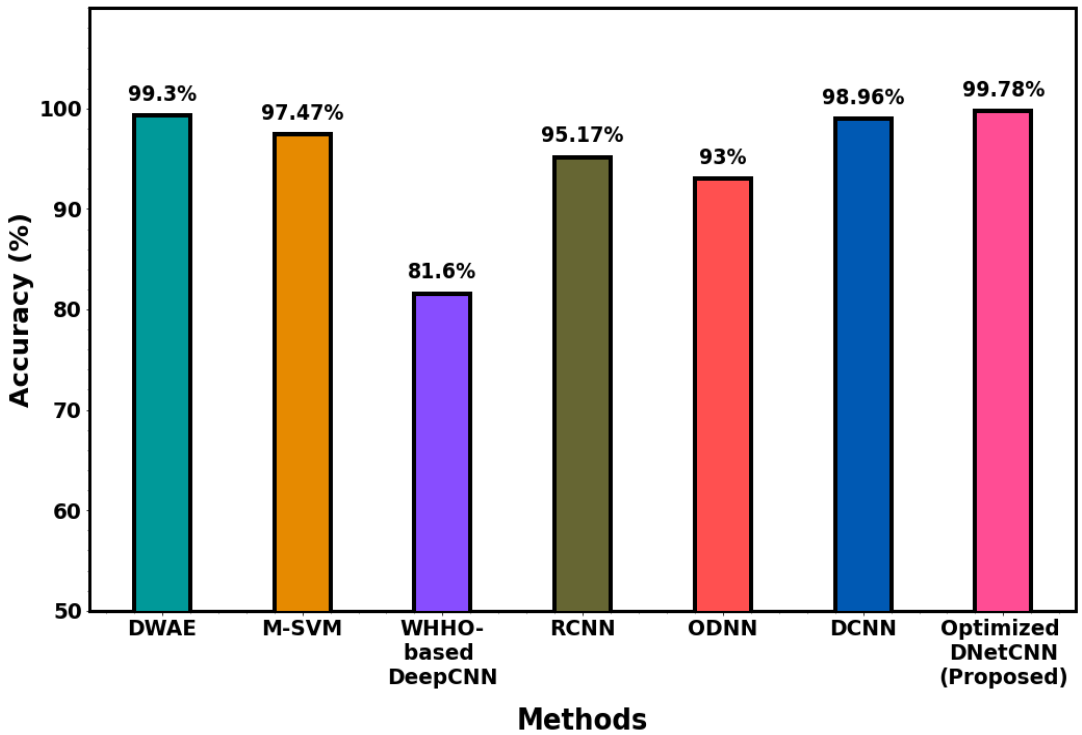

Fig. 8. An overall comparison of previous with proposed technique in literature.

Fig. 8 illustrates the comparison outcome of the proposed with previous approaches in the literature. A confusion matrix is a performance-measuring tool used in statistics and deep learning to assess a categorization model's effectiveness. It is a table that, when compared to the actual ground truth labels, provides a summary of the model's predictions, enabling the performance of an algorithm to be visually represented.

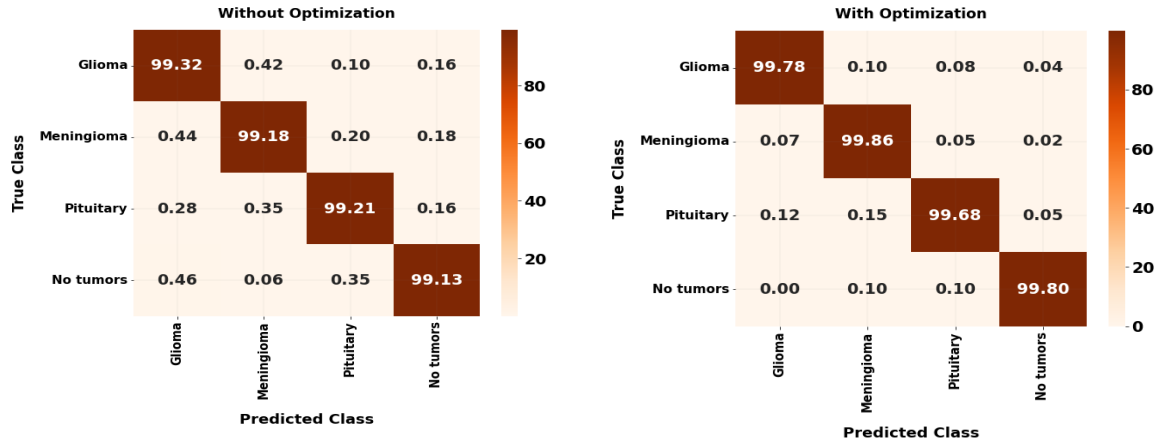

(a) (b)

Fig. 9. Confusion matrix for without optimization and with optimization.

Fig. 9 shows the confusion matrix with and without the optimization algorithm.

4.6. Training and Testing Evaluation

The main purpose of training accuracy and loss is to direct the model's learning process. Testing and training accuracy as well as testing and training loss functions are shown in Fig. 10, which offers insights into how well the model would probably perform on fresh, untested data.

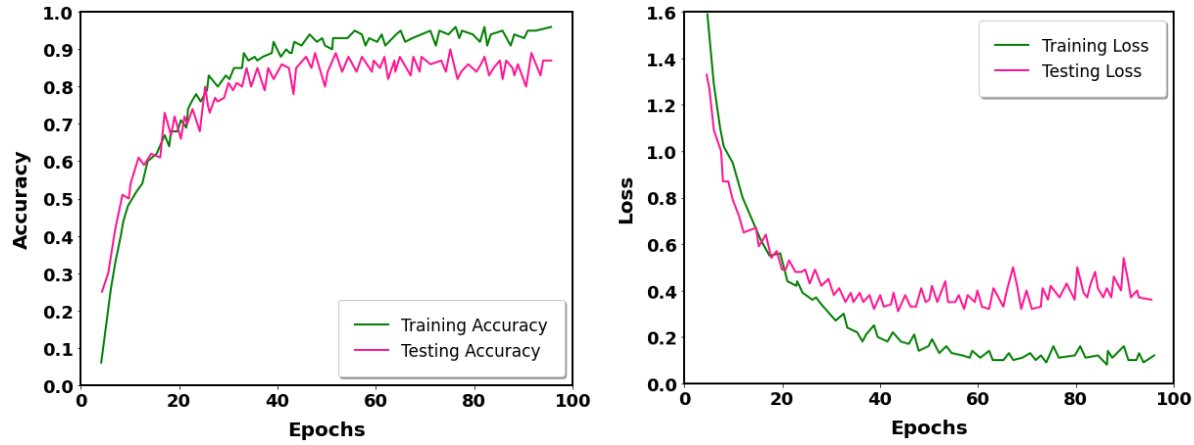

(a) (b)

Fig. 10. Simulation of testing and training, (a) Accuracy, (b) Loss on the dataset.

During the training stage, the proposed approach is taught using the prepared training set for 100 epochs. A 0.1 learning rate has been established.

4.7. Computational Time

The complexity size of the dataset, the deep learning approaches utilized, the attributes chosen for classification, and the available sources are some of the attributes that affect the computational complexity of brain disease categorization.

Table 5. Overall comparison of proposed and existing methods for computational time.

Reference	Method	Computational Time (ms)
Shuai et al. [16]	DWAE	0.43
Maqsood et al. [17]	M-SVM	0.27
Rammurthy & Mahesh [18]	WHHO-based DeepCNN	0.37
Vankdothu & Hameed [19]	RCNN	0.32
Preethi & Aishwarya [20]	ODNN	0.26
Aurna et al. [21]	DCNN	0.23
Proposed Method	Optimized DNetCNN	0.18

The process of accurately classifying individuals into various illness categories, such as brain tumours, usually entails the study of medical imaging data, such as MRI or fMRI scans. Table 5 illustrates a summary of the calculation times for the proposed and previous approaches.

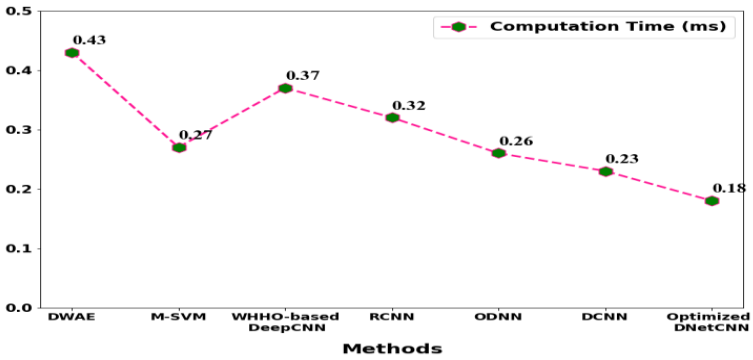

Fig. 11. The overall computational time comparison of proposed and previous approaches.

The entire computing time comparison between the proposed approach and the current methods is shown in Fig. 11. When compared to existing techniques, the proposed approach operates with reduced computing time.

5. CONCLUSION

To achieve high classification accuracy in a short amount of time, a Darknet Convolutional Neural Network design is proposed for the detection of gliomas, meningiomas, and normal, and pituitary brain disorders. A suitable brain tumour dataset is necessary first to carry out the training and testing procedure quickly. Second, the MRI images were pre-processed in two steps: the MRI images were denoised, and the contrast of the images was improved. Third, we train our model from scratch using the desired patterns as part of a training approach. Fourth, we employed the proposed model to effectively extract characteristics from the MRI pictures and classify them. We assess the proposed framework using a dataset of MRI pictures. The accuracy of the proposed model was 99.78% overall. When compared to existing methods, the proposed approach achieved higher categorization accuracy with less computational time complexity. To raise the proposed model's accuracy, plan to add more MRI pictures to the dataset in the future. Furthermore, expanding on this idea for future research could involve applying the proposed approach to other kinds of medical pictures, like computed tomography, ultrasound, and X-rays.

Declarations

Competing Interests: The authors declare that they have no known competing financial interests or personal relationships that could have appeared to influence the work reported in this paper.

Data Availability Statements: Data will be available when requested

Authors' Contributions: The author confirms sole responsibility for the following: study conception and design, data collection, analysis and interpretation of results, and manuscript preparation.

Funding: No funding was received to assist with the preparation of this manuscript.

Ethics Approval: This material is the author's original work, which has yet to be previously published elsewhere. The paper reflects the author's research and analysis truthfully and completely.

REFERENCES

[1]. Pedada, K. R., Rao, B., Patro, K. K., Allam, J. P., Jamjoom, M. M., & Samee, N. A. 2023,A novel approach for brain detection using deep learning-based technique. Biomedical Signal Processing and Control, 82, 104549.

[2]. Dr.A. Muthusamy, Dr.S. Maheswari, Dr.S. Anitha, Dr.C.P. Selvi, Dr.N. Vanitha, Dr.G. Saravanan, ,2025,An Enhanced Model Of Efficient net Convolution Neural Networks (Cnns) To Predict Brain Tumor Segmentation. International Journal of Environmental Sciences. 862-871. 10.64252/nfxy2057.

[3]. Nanda, A., Barik, R. C., & Bakshi, S.2023, "SSO-RBNN driven brain tumor classification with Saliency-K-means segmentation technique". Biomedical Signal Processing and Control, 81, 104356.

[4]. Monika Agarwal, Geeta Rani, Ambeshwar Kumar, Pradeep Kumar K, R. Manikandan, Amir H. Gandomi,2024,"Deep learning for enhanced brain Tumor Detection and classification", Results in Engineering, Volume 22.

[5]. Vijendar, A., Madhavi, P., Kumar, K. S., & Boga, J,2025 "Advancing Healthcare With Deep Learning: Innovations In Medical Image Analysis. International Journal of Environmental Sciences", 11(18s).

[6]. E. Irmak,2021, Multi-classification of brain tumour MRI images using a deep convolutional neural network with fully optimized framework," Iranian Journal of Science and Technology Transactions of Electrical Engineering, vol. 45, no. 3, pp. 1015-1036.

[7]. A. Raza, H. Ayub, J. A. Khan, I. Ahmad, A. S. Salama, Y. I. Daradkeh and H. Hamam, 2022,"A hybrid deep learning-based approach for brain tumour classification," Electronics, vol. 11, no. 7, pp. 1146.

[8]. F. J. Díaz-Pernas, M. Martínez-Zarzuela, M. Antón-Rodríguez and D. González-Ortega,2021, "A deep learning approach for brain tumour classification and segmentation using a multiscale convolutional neural network," In Healthcare, vol. 9, no. 2, pp. 153.

[9]. M. I. Sharif, M. A. Khan, M. Alhussein, K. Aurangzeb and M. Raza,2021, "A decision support system for multimodal brain tumour classification using deep learning," Complex & Intelligent Systems, vol.1, pp. 1-14.

[10]. M. Aamir, Z. Rahman, Z. A. Dayo, W. A. Abro, M. I. Uddin, I. Khan and Z. Hu, 2022,"A deep learning approach for brain tumour classification using MRI images," Computers and Electrical Engineering, vol. 101, pp. 108105.
[11]. T. Tazin, S. Sarker, P. Gupta, F. I. Ayaz, S. Islam, M. Monirujjaman Khan and H. Alshazly, 2021,"A robust and novel approach for brain tumour classification using convolutional neural network," Computational Intelligence and Neuroscience, vol.1, pp. 1-34.
[12]. C. S. Rao and K. Karunakara,2022, "Efficient detection and classification of brain tumors using kernel based SVM for MRI," Multimedia Tools and Applications, vol. 81, no. 5, pp. 7393-7417.
[13]. N. Kesav and M. G. Jibukumar, 2022,"Efficient and low complex architecture for detection and classification of Brain Tumor using RCNN with Two Channel CNN," Journal of King Saud University-Computer and Information Sciences, vol. 34, no. 8, pp. 6229-6242.
[14]. C. Öksüz, O. Urhan and M. K. Güllü, 2022,"Brain tumour classification using the fused features extracted from expanded tumour region," Biomedical Signal Processing and Control, vol. 72, no.1, pp. 103356.
[15]. S. A. Qureshi, S. E. A. Raza, L. Hussain, A. A. Malibari, M. K. Nour, A. U. Rehman and A. M. Hilal, 2022,"Intelligent ultra-light deep learning model for multi-class brain tumour detection," Applied Sciences, vol. 12, no. 8, pp. 3715.
[16]. I. Abd El Kader, G. Xu, Z. Shuai, S. Saminu, I. Javaid, I. S. Ahmad and S. Kamhi, 2021,"Brain tumour detection and classification on MR images by a deep wavelet auto-encoder model," Diagnostics, vol. 11, no. 9, pp. 1589.
[17]. S. Maqsood, R. Damaševičius and R. Maskeliūnas,2022, "Multi-modal brain tumour detection using deep neural network and multiclass SVM," Medicina, vol. 58, no. 8, pp. 1090.
[18]. D. Rammurthy and P. K. Mahesh, 2022,"Whale Harris hawks optimization based deep learning classifier for brain tumour detection using MRI images," Journal of King Saud University-Computer and Information Sciences, vol. 34, no. 6, pp. 3259-3272.
[19]. R. Vankdothu and M. A. Hameed, 2022,"Brain tumour MRI images identification and classification based on the recurrent convolutional neural network," Measurement: Sensors, vol. 24, no. 1, pp. 100412.
[20]. S. Preethi and P. Aishwarya, 2021,"An efficient wavelet-based image fusion for brain tumour detection and segmentation over PET and MRI image," Multimedia Tools and Applications, vol. 80, no. 10, pp. 14789-14806.
[21]. N. F. Aurna, M. A. Yousuf, K. A. Taher, A. K. M. Azad and M. A. Moni, 2022,"A classification of MRI brain tumour based on two stage feature level ensemble of deep CNN models," Computers in biology and medicine, vol. 146, no. 1, pp. 105539.